Biosensors and Bioelectronics 141 (2019) 111283

Contents lists available at ScienceDirect

Biosensors and Bioelectronics

journal homepage: www.elsevier.com/locate/bios

Wireless power transfer analysis of circular and spherical coils under misalignment conditions for biomedical implants

Yellappa Palagani, Krithikaa Mohanarangam, Jae Hoon Shim, Jun Rim Choi*

School of Electronics Engineering, College of IT Engineering, Kyungpook National University, Daegu, 702-701, South Korea

ARTICLE INFO

Keywords:
IMD'S
3-Coil inductive WPT system
Spherical
Circular
Misalignment issue
PTE
Three-layered human tissue

ABSTRACT

In this paper, a 3-coil inductive WPT system having circular shaped external coil and miniaturized spherical shaped implantable coil is designed and optimized at 13.56 MHz to overcome reduced PTE under misalignment conditions. The external coil is placed at a distance of 10 mm from the implantable coil. The proposed design is referred to as C–S WPT system. To evaluate the performance of the C–S WPT system, a 3-coil inductive WPT system having circular shaped external coil and circular shaped implantable coil is designed and is referred to as C–C WPT system. The impacts of perfect alignment, lateral and/or angular misalignments on the overall PTE of the systems are analyzed and compared. At perfect alignment, the PTE of C–C and C–S WPT systems are 59.8% and 52.6%, respectively. Though the PTE of C–C WPT system is slightly higher than C–S WPT system, there is a sharp decrease in PTE of C–C system for angles greater than 40°. At 90° of angular misalignment, the PTE's of C–C and C–S WPT systems are 0.4% and 5.6% respectively. When the coils are laterally displaced by a distance of 10 mm, the C–C and C–S WPT systems produce PTE of 33.4% and 27.1% respectively. The C–C and C–S WPT systems attain PTE of 1.6% and 5.5% respectively at 10 mm displacement and 50° rotation. The simulated systems are fabricated to analyze the result in real-environment. The measurement results show that the C–S WPT system provides better PTE when compared to C–C WPT system under angular and a combination of angular and lateral misalignments.

1. Introduction

Implantable medical devices (IMD's) such as cochlear implants (HG et al., 2009), retinal prostheses (Stingl et al., 2013), cardiac pacemakers (Das and Yoo, 2015), brain machine interfaces (Lee et al., 2013), and neuromuscular stimulators (Kassiri et al., 2017) remain popular in biomedical applications as these devices allow precise monitoring of physiological activity, drug delivery, and local stimulation. Powering the IMD's is a matter of utmost importance and the power level should range from a few microwatts to tens of milliwatts (Poon et al., 2007; RamRakhyani et al., 2011; Arbabian et al., 2016; Agarwal et al., 2017; Agrawal et al., 2017). The conventional techniques used physical wirings or batteries to provide power to the IMD's, however, the process exhibited several disadvantages (RamRakhyani et al., 2011; Agrawal et al., 2017). Wireless power transfer (WPT) technology in IMD's is proved to be safe and reliable alternative to wires and batteries (Agarwal et al., 2017; Agrawal et al., 2017; Jow and Ghovanloo, 2007; Lenaerts and Puers, 2007; Carta et al., 2009). An efficient WPT system should be able to transfer the power required by the implantable coil at both perfectly aligned and misaligned scenarios. To achieve the required power transfer efficiency (PTE) at perfect and misalignment scenarios, it is important to choose the right WPT configuration, size, shape, and distance between the coils. Furthermore, the impact of the operating frequency on specific absorption rate (SAR) must be investigated to ensure specified safety standards set by Federal Communications Commission (FCC) are met (Jia et al. 2017).

Inductively coupled transmitter and receiver coils were used initially to power the IMD's (Jow and Ghovanloo, 2007). The PTE of such a system depends largely on the coupling between the coils and their quality factor (Q-factor). Increasing the distance between the coils lead to a precipitous drop in the coupling coefficient thereby decreasing the overall PTE. Thus, this system works well only when the coils are not too far away from each other. By overcoming the disadvantages of the 2-coil inductive link, 4-coil resonance-based link operating in the midfield region have gained popularity over the past few years (RamRakhyani et al., 2011; Karalis et al., 2008; Khan and Choi, 2016). The coupling coefficient, Q-factor and overall PTE of a 4-coil resonance-based link are high compared with the conventional 2-coil inductive link. Although the PTE of a 4-coil resonance-based WPT system is high, the power delivered to load (PDL) is low. This drawback can be

* Corresponding author.
E-mail address: jrchoi@knu.ac.kr (J.R. Choi).

https://doi.org/10.1016/j.bios.2019.04.051
Received 14 December 2018; Received in revised form 11 April 2019; Accepted 24 April 2019
Available online 11 May 2019
0956-5663/

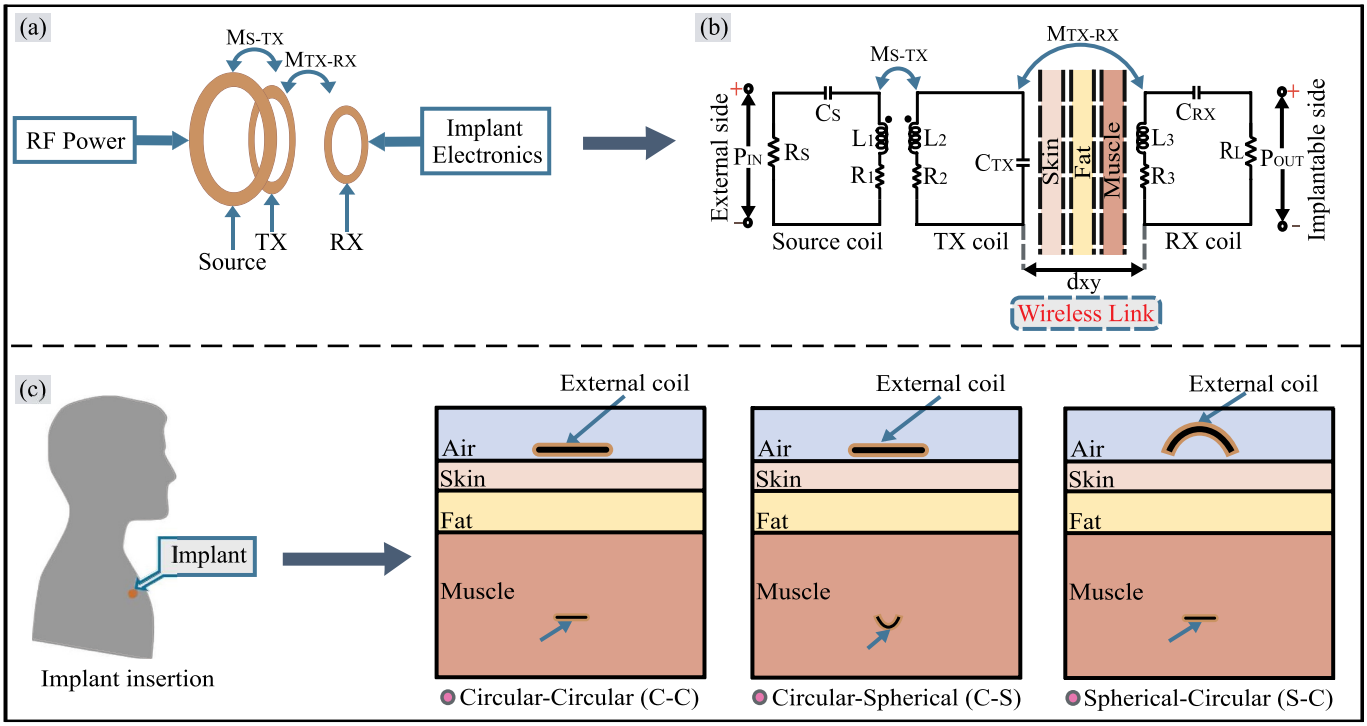

Fig. 1. (a) Block diagram of a 3-coil inductive link. (b) The equivalent circuit model of a 3-coil inductive link. (c) The orientation of the external and implantable coils of 3-coil inductive WPT systems at three-layered human tissue medium.

overcome by a 3-coil inductive WPT link and therefore in this study, a 3-coil inductive WPT link as shown in Fig. 1 (a) and (b) is considered (Kiani et al., 2011; Mirbozorgi et al., 2012; Zhong et al., 2015; Zhang et al., 2017).

The size and shape of the coils are imperative for attaining maximum PTE between the coils. Here, the size of the implantable coil is chosen based on the operating frequency (Ahn and Ghovanloo, 2016). According to the FCC for Industrial Scientific and Medical (ISM) applications, a frequency of less than 20 MHz has nil or lesser effects on the tissues of a human (Jia et al. 2017). Considering this fact, in this paper, 13.56 MHz is chosen to be the operating frequency to avoid the adverse effects on human tissue. The methods of the past had used circular and rectangular shaped coils to achieve higher PTE at various alignments (RamRakhyani et al., 2011; Jow and Ghovanloo, 2007; Khan and Choi, 2016; Kiani et al., 2011; Nguyen et al., 2014; Chatterjee et al., 2017). Though these systems produce a high PTE at perfect alignment, the PTE at misalignment scenarios is very low (Khan and Choi, 2016; Nguyen et al., 2014). We have proposed a 3-coil inductive methodology by employing spherical shaped implantable coil to overcome the drawbacks of these conventional shapes. The maximum implantation depth between the external and implantable coils is 10 mm (Jow and Ghovanloo, 2007; Khan and Choi, 2016; Mutashar et al., 2014). The daily activities like breathing and motion of a human being can lead to misalignment of coils, thereby reducing the PTE. So, it is important to examine and compare the performance of the coils at perfect and misalignment scenarios. This paper analyzes the impacts of perfect alignment, lateral and/or angular misalignments on the overall PTE of the system. First, the system is designed with air in between the coils and to analyze the system in real-environment, a three-layered human tissue made by layers of skin, fat, and muscle as shown in Fig. 1(c) is designed as a medium between the external and implantable coils.

In this paper, a 3-coil inductive WPT system having a spherical shaped implantable coil at a distance of 10 mm from the circular shaped external coil is designed at 13.56 MHz to investigate the impacts of perfect alignment, lateral and/or angular misalignments on the overall PTE of system. A 3-coil inductive WPT system having circular shaped external and implantable coils is also designed to evaluate the performance of the proposed system with the conventional works. The percentage of skin, fat and muscle varies from person to person, therefore, the PTE is analyzed for various tissue compositions in tissue medium. In the following section, the equivalent circuit of a 3-coil inductive link and orientation of the coils are discussed. The optimization procedure and simulation results of the designed systems are described in Section 3. Section 4 shows the measurement results, followed by the conclusion Section.

2. Simplified equivalent model and orientation analysis of a 3-coil inductive link

2.1. Equivalent circuit model of a 3-coil inductive link

The 3-coil inductive link, an extension of the conventional 2-coil inductive link is shown in Fig. 1(b). Adding an additional coil to a 2-coil inductive WPT system improves the PTE of the system. For this reason, here, an additional source coil (L_S) is added to the transmitter coil (L_{TX}) of a 2-coil system. The high-Q L_{TX} is strongly coupled with the L_S. These strongly coupled coils, in turn, are mutually coupled with the receiver coil (L_{RX}). L_1, L_2, L_3 and R_1, R_2, R_3 are the self-inductances and self-resistances of L_S, L_{TX} and L_{RX} respectively. R_S and R_L are the source resistance and load resistance of the system. C_S, C_{TX} and C_{RX} are the capacitances of L_S, L_{TX} and L_{RX} respectively. The resonance frequency of the coils is tuned to the operating frequency by varying C_S, C_{TX} and C_{RX}. d_{xy} denotes the distance between the external coil and implantable coil of the system. The three coils are linked to each other via a magnetic field characterized by the mutual inductances M_{S-TX} and M_{TX-RX}. The mutual inductance M_{xy} ($x, y \in \{1,2,3\}$) can be expressed as in (equation 1).

$$M_{xy} = k_{xy}\sqrt{L_x L_y} \qquad (0 < k < 1), \tag{1}$$

where L_x and L_y are the self-inductance of the coils x and y respectively, and k_{xy} is the coupling coefficient between them. The Q-factor (Q_{xy}),

plays a vital role in achieving a high PTE. Q_{xy} of the coils can be expressed as

$$Q_{xy} = f_r/\Delta_f \quad (2)$$

where f_r and Δf are the resonance frequency and bandwidth of the WPT system respectively. The overall PTE of the system in terms of s-parameter can be expressed as (Jia et al. 2017; Vijayakumaran Nair and Choi, 2016)

$$\text{PTE} = |S_{21}'|^2 \times 100(\%) \quad (3)$$

where $|S_{21}'|$ is the linear magnitude of the transmission coefficient.

2.2. External and implantable coils at perfect and misalignment cases

The orientation of the external and implantable coils directly impact PTE of the system (Soma et al., 1987). Therefore, this paper investigates the impacts of perfect alignment, lateral and/or angular misalignments on the overall PTE of the 3-coil inductive system. Generally, the PTE is high only in the best-case scenario, i.e., perfect alignment. In several misalignment scenarios, the PTE decreases and power cannot be successfully transferred to the implantable coil. The various scenarios include I) Perfect alignment: Here $\Delta = 0$ mm and $\alpha = 0°$, where Δ is the displacement and α is the angular rotation. In this alignment, the implantable coil is parallel to the external coil. In general, this alignment allows maximum power transfer between the coils. II) Angular misalignment: The implantable coil rotates at an angle greater than 0°, i.e., $\Delta = 0$ mm and $\alpha \neq 0°$. III) Lateral misalignment: The implantable coil is laterally displaced i.e., $\Delta \neq 0$ mm and $\alpha = 0°$. IV) Combination of lateral and angular misalignment: In this scenario, the implantable coil laterally shifts and rotates i.e., $\Delta \neq 0$ mm and $\alpha \neq 0°$. The orientation of the coils at the above discussed cases are presented in Fig. 2(a), (b), and (c).

3. Optimization procedure of 3-coil inductive link

Fig. 2(d) depicts the iterative procedure for designing a 3-coil inductive link which starts with a set of design constraints and parameters and ends with optimized design parameters for attaining a maximum PTE between the coils (Kiani et al., 2011). The parameters required to begin the iterative procedure are r_{out} (outer radius of the coils), d_{xy}, shape of the coils and medium between the coils. Firstly, a set of design constraints and parameters are initialized and coils are analyzed at perfect alignment. Secondly, the resulting optimized design constraints and parameters are further used in analyzing the coils under various misalignment scenarios. This design is simulated at a frequency of 13.56 MHz with 10 mm as target distance.

Step-1: Assign design constraints: The implantable coil has size constraints as it is placed inside the human body. Therefore, r_{outLRX} has to be set in a way that the coil can be easily fabricated. The design constraints are set to meet the requirement of the application and fabrication process. Conventional methods have employed circular and rectangular shaped external and implantable coils. These coils misalign due to various external and internal factors because of which the PTE drops steeply (Gong et al., 2017; Khan and Choi, 2016; Nguyen et al., 2014). The overall PTE of the design can be improved by using a spherical shaped coil. But a spherical coil at the external side is ineffectual as the d_{xy} increases with increase in size and height as a result of which the PTE drops drastically at perfect alignment (Yellappa et al., 2018). The authors have designed a spherical shaped external and circular shaped implantable coils called as S–C WPT system to show the drawbacks of using a spherical coil in the external side. A C–S WPT system having a spherical coil at the implantable side and circular coil at the external side is designed and compared to the conventional C–C WPT system which has circular shaped external and implantable coils.

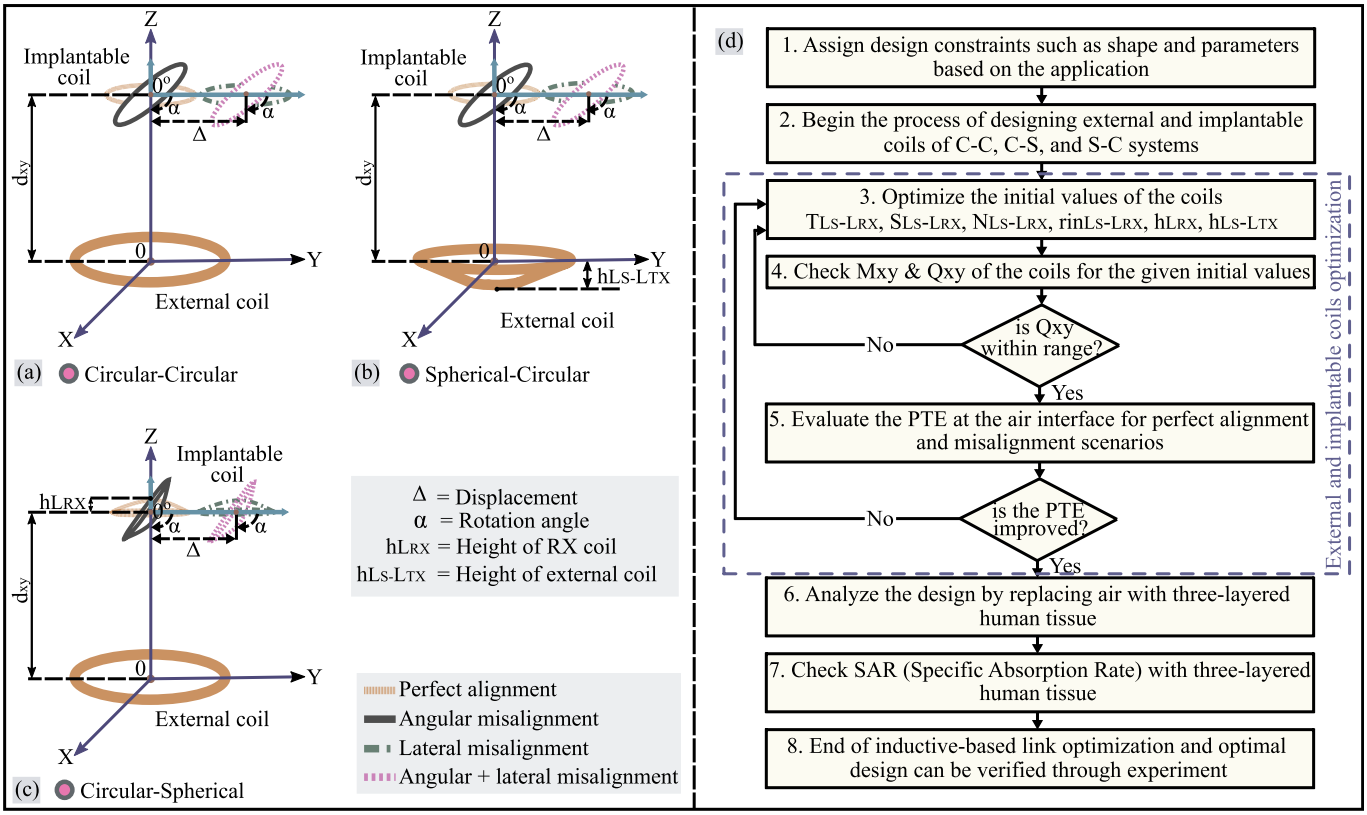

Fig. 2. (a), (b), and (c) Orientation of the external and implantable coils in C–C, S–C, and C–S WPT systems. (d) Optimization procedure flowchart of 3-coil inductive link design.

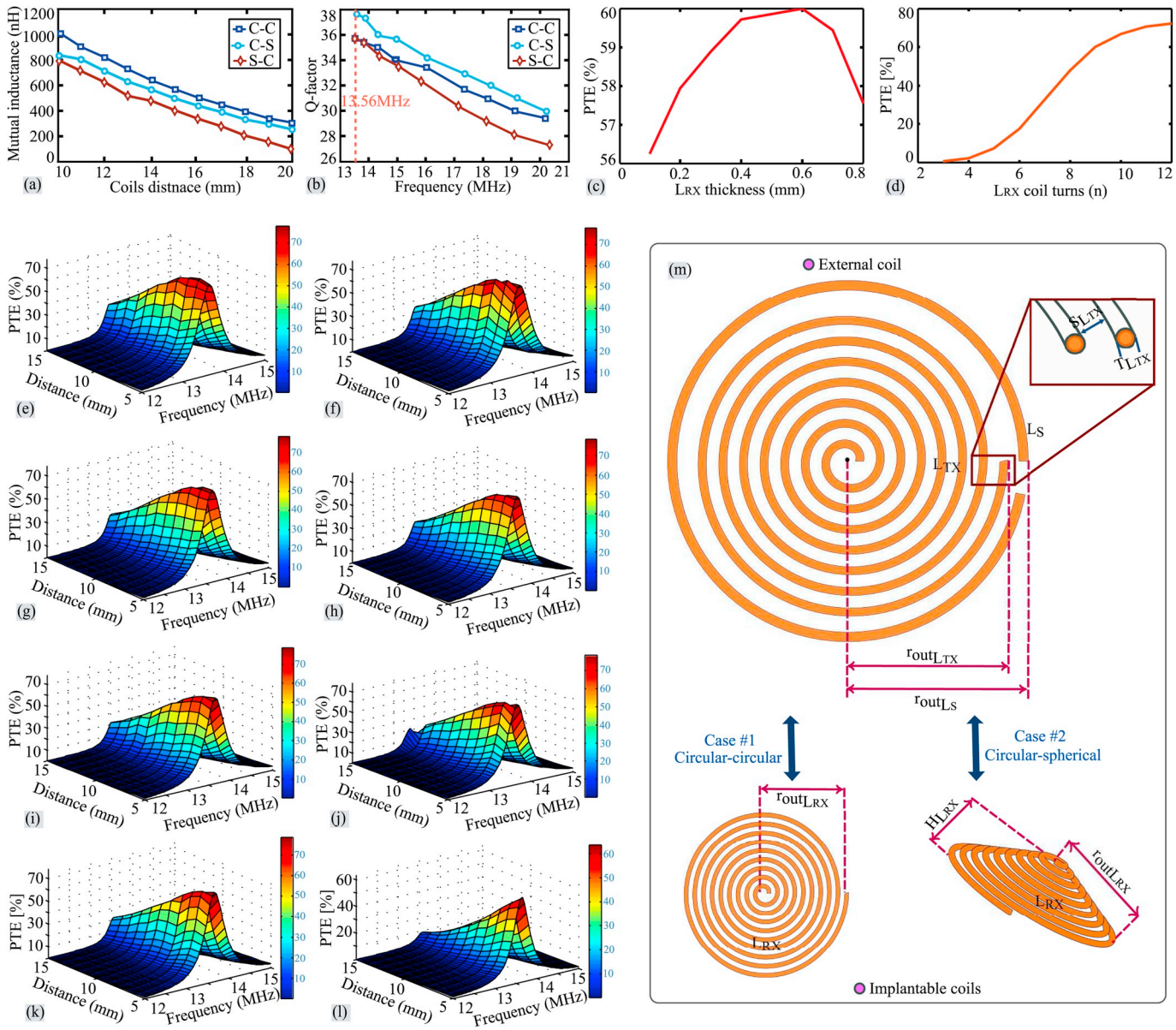

Fig. 3. (a) Mutual inductance vs d_{xy}. (b) Q-factor variation vs frequency. (c) PTE vs L_{RX} thickness. (d) PTE vs L_{RX} turns. (e) PTE vs frequency vs d_{xy} of C–C system. (f), (g), (h), (i), (j), and (k) represents PTE vs frequency vs d_{xy} of C–S system with L_{RX} height of 0.9 mm, 1.8 mm, 2.7 mm, 3.6 mm, 4.5 mm, and 5.4 mm respectively. (l) PTE vs frequency vs d_{xy} of S–C system. (m) C–C (case#1) and C–S (case#2) geometry coil types.

Step-2: Begin the coil design procedure: Here, considering the design constraints assigned in *step* − 1, the procedure for designing the external and implantable coils of C–C, C–S, and S–C systems is initialized.

Step-3: Assign and optimize the initial values: The initial parameters are defined for designing L_S, L_{TX} and L_{RX} of the C–C, C–S and S–C WPT systems. These parameters are T_{LS-LRX} (copper wire thickness), S_{LS-LRX} (spacing between the wires), N_{LS-LRX} (number of turns in a coil), $r_{inLS-LRX}$ (inner radius of the coil), h_{LRX} (height of the spherical shaped implantable coil) and h_{LS-LTX} (height of the spherical shaped external coil).

Step-4: Mutual inductance and quality factor: Here, M_{xy} and Q_{xy} are optimized through simulation. Optimizing N_{LS-LRX}, T_{LS-LRX}, and S_{LS-LRX} improves the M_{xy} and Q_{xy}, so *Step-3* is repeated iteratively if Q_{xy} and M_{xy} fail to fall within the expected range. The higher the value of Q_{xy} and M_{xy}, the higher the value of PTE. The optimized parameters for designing C–C, C–S and S–C WPT systems are tabulated in Fig. 5(a). To tune the operating frequency to resonance frequency, we have varied the capacitance across the external and implantable coils of C–C, C–S and S–C WPT systems individually. The C_S, C_{TX} and C_{RX} of C–C WPT system are 425 pF, 280 pF, and 400 pF respectively, and that of C–S WPT system are 425 pF, 279.5 pF, and 400 pF respectively. The C_S, C_{TX}, and C_{RX} of S–C WPT system are 425 pF, 262 pF, and 400 pF respectively. The impedance of the L_S and L_{RX} are set to 50Ω. At 13.56 MHz, the Q_{xy} and M_{xy} of the C–C WPT system are 35.6 and 1018.44 nH respectively. The Q_{xy} and M_{xy} of the C–S WPT system are 37.6 and 835.43 nH respectively, and that of S–C WPT system are 35.6 and 798.85 nH respectively. The M_{xy} and Q_{xy} of the C–C, C–S, and S–C systems with respect to frequency and coil distance are shown in Fig. 3(a) and (b) respectively.

Step-5: Evaluation of PTE at air as interface under perfect alignment and misalignment scenarios: The PTE is evaluated considering the obtained design parameters. For a low PTE, *Step-3* is repeated iteratively as optimizing the initial parameters improves the Q_{xy} and M_{xy}, which in turn increases the PTE of the system. The number of turns

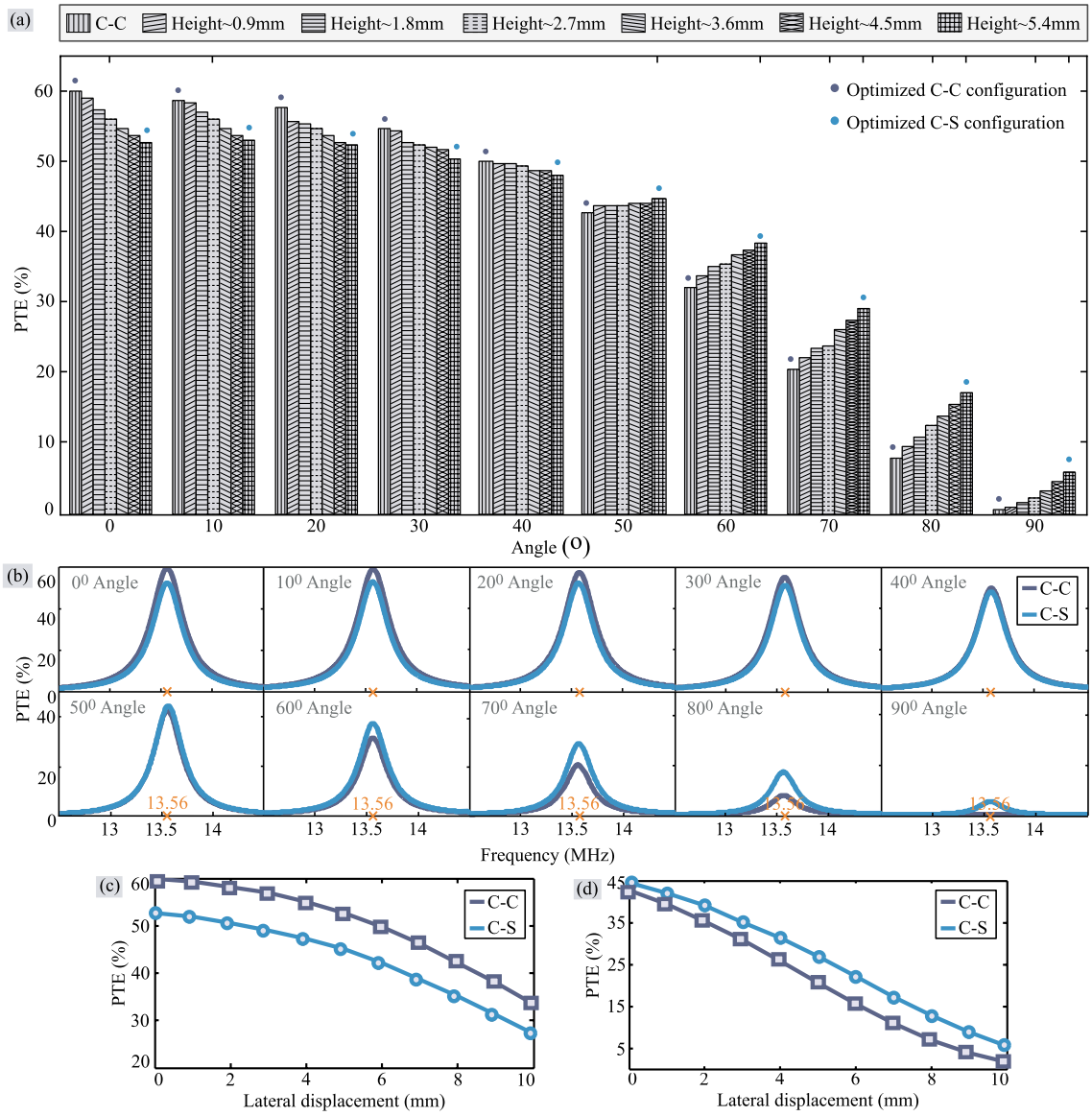

Fig. 4. (a) PTE vs angle of rotation for C–C and C–S systems (0° → 90°). (b) PTE vs frequency for C–C and C–S systems. (c) PTE of the coils at lateral misalignment. (d) PTE of the coils at 50° of angular and lateral misalignment.

in a L_{RX} must be effectively optimized as it is implanted inside the human body. In this paper, the optimized diameter of the L_{RX} in C–C and C–S WPT systems is 1.88 cm. It can be observed from Fig. 3(c) and (d) that the C–C and C–S WPT systems are able to achieve PTE's of 59.8% and 52.6% respectively by optimizing $T_{L_{RX}}$ to 0.6 mm and $N_{L_{RX}}$ to 9. The PTE of the S–C WPT system is 30.1%, which is exceptionally low and therefore only C–C and C–S WPT systems are further analyzed and compared. The effects of d_{xy} on the PTE of C–C and C–S WPT systems are investigated. The results show that the PTE decreases gradually with increasing d_{xy}. The change in PTE with respect to distance and frequency of C–C WPT system can be observed in Fig. 3(e). Fig. 3(f), (g), (h), (i), (j), and (k) represent the PTE of C–S WPT system with respect to distance and frequency at different implantable coil heights. Fig. 3(l) represents the PTE of S–C WPT system with respect to distance and frequency. Fig. 3(m) shows the geometric structure of C–C and C–S coil designs.

Step-5.1: Misalignment analysis: The simulated results of C–C and C–S WPT systems at various coil misalignment scenarios are presented below.

Step-5.1.1: Angular misalignment: The implantable coil rotates through different angles, where the maximum angle of rotation is 90°. The PTE is calculated at 0°, 10°, 20° …. , 90° of angular misalignment. As mentioned above, the C–C and C–S systems produce PTE of 59.8% and 52.6% at perfect alignment. When the implantable coil is rotated through an angle 90° (worst-case scenario) along the y-axis, the C–C and C–S systems produce PTE of 0.4% and 5.6% respectively. Fig. 4(a) shows the PTE at various angles of rotation and Fig. 4(b) shows PTE at various angles of rotation with respect to frequency. Though the PTE of C–C system is slightly higher than C–S system, there is a sharp decrease in PTE of C–C system for angles greater than 40°.

Step-5.1.2: Lateral misalignment: To validate the system at worst-case scenario, 10 mm is considered to be the maximum distance of misalignment. The implantable coil is moved laterally and the center of the coil is displaced by a distance of 1 mm, 2 mm, 3 mm …, 10 mm and the PTE at each of these lateral misaligned distances are calculated. At the worst-case, the PTE of the C–C and C–S systems are 33.4% and 27.1% respectively. Fig. 4(c) shows the PTE with respect

(a)

PHYSICAL PARAMETERS				
Coils	**Symbols**	**C-C**	**C-S**	**S-C**
L_S	r_{inL_S}(mm)	26.5	26.5	26.5
	r_{outL_S}(mm)	27.5	27.5	27.5
	T_{L_S}(mm)	2	2	2
	N_{L_S}	1	1	1
	h_{L_S}(mm)	-	-	8
L_{TX}	$r_{inL_{TX}}$(mm)	1.75	1.75	1.75
	$r_{outL_{TX}}$(mm)	24.02	24.02	24.02
	$T_{L_{TX}}$(mm)	1.7	1.7	1.7
	$S_{L_{TX}}$(mm)	1.41	1.41	1.41
	$N_{L_{TX}}$	7	7	7
	$h_{L_{TX}}$(mm)	-	-	7
L_{RX}	$r_{inL_{RX}}$(mm)	0.6	0.65	0.6
	$r_{outL_{RX}}$(mm)	9.36	9.41	9.36
	$T_{L_{RX}}$(mm)	0.6	0.6	0.6
	$S_{L_{RX}}$(mm)	0.34	0.34	0.34
	$N_{L_{RX}}$	9	9	9
	$h_{L_{RX}}$(mm)	-	5.4	-
	Distance (mm)	d_{xy}	10	
	Operating frequency (MHz)	f_0	13.56	
	Wire type		Copper	

(b)

	Air	Dry skin	Wet skin	Fat	Muscle
Conductivity [S/m]	0	0.23802	0.38421	0.030354	0.62818
Relative permittivity	1	285.25	177.13	11.827	138.44
Loss tangent	0	1.1062	2.8754	3.4021	6.0152

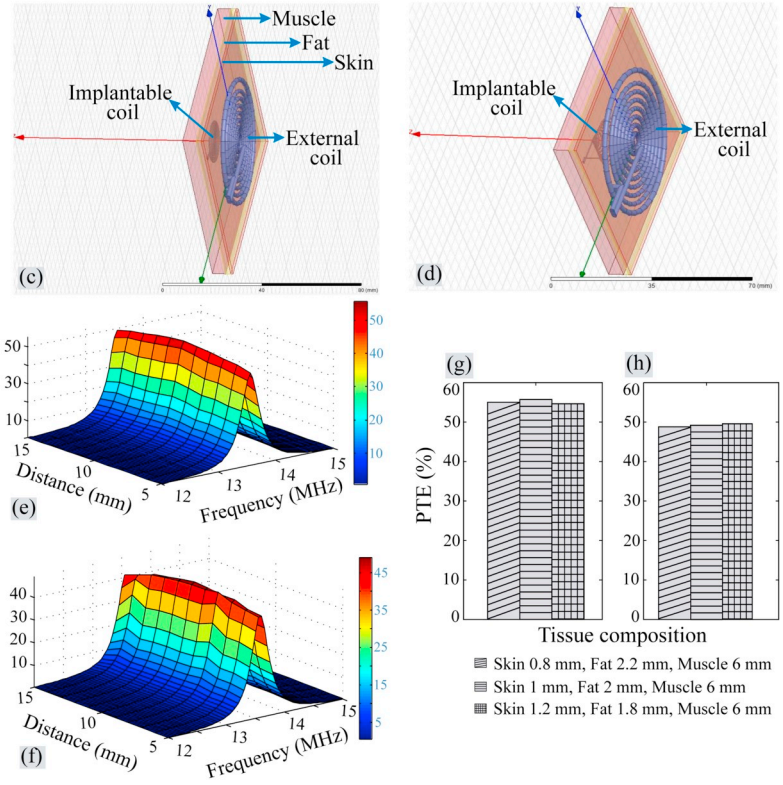

Fig. 5. (a) Optimized geometries for C–C, C–S, and S–C coil designs. (b) The dielectric properties of the human body tissue at 13.56 MHz. (c) C–C WPT system at three-layered human tissue. (d) C–S WPT system at three-layered human tissue. (e) PTE of C–C WPT system vs frequency vs d_{xy}. (f) PTE of C–S WPT system vs frequency vs d_{xy}. (g) PTE vs tissue composition of C–C WPT system. (h) PTE vs tissue composition of C–S WPT system.

to the misaligned distances mentioned above and it can be observed that even under worst-case scenario, the difference between the PTE at perfect alignment and lateral misalignment of C–C and C–S systems are almost the same.

Step-5.1.3: Combination of angular and lateral misalignment: Here, the coils undergo both lateral and angular misalignments. It can be observed from Fig. 4(d) that when the implantable coil is rotated through an angle greater than 40° and displaced by a distance greater than 0 mm, the PTE of the C–S system is found to be better than the C–C system. For an example, when the coil is rotated through an angle of 50° and laterally displaced by a distance of 10 mm, the C–C and C–S produced PTE of 1.6% and 5.5% respectively. Fig. 4(d) shows the PTE of the systems at a combination of angular and lateral misalignments.

Step-6: PTE at three-layered tissue medium: This step analyzes the PTE of C–C and C–S systems through different compositions of tissue in between the coils. To analyze the design in real-environment, the human tissue model is formed using 1 mm of skin, 2 mm of fat and 6 mm of muscle by considering the dielectric properties of the tissue shown in Fig. 5(b) (https://www.fcc.gov/general/body-tissue-dielectric-parameters). Fig. 5(c) and (d) show the designed human tissue models of the C–C and C–S WPT systems. The skin layer in the human tissue model is created by considering two types of skin, namely, dry skin and wet skin. The PTE of the tissue model having dry skin and wet skin in C–C system are 55.8% and 55.7% respectively whereas for C–S WPT system are 49.3% and 49.2%. respectively. Since the PTE of both the skin types are almost the same, the wet skin tissue is selected for further analysis. The PTE of C–C and C–S WPT systems at three-layered tissue medium with respect to distance and frequency are shown in Fig. 5(e) and (f). The percentage of skin, fat and muscle varies from person to person, therefore, in addition to 1 mm of skin, 2 mm of fat and 6 mm of muscle, the human tissue model is also formed using 0.8 mm of skin, 2.2 mm of fat and 6 mm of muscle and 1.2 mm of skin, 1.8 mm of fat and 6 mm of muscle. Fig. 5(g) and (h) show the effects of different tissue compositions on PTE of C–C and C–S systems and it can be observed that the PTE attained are almost the same regardless of tissue compositions.

Step-7: SAR (Specific absorption rate): SAR is directly proportional to tissue conductivity (σ) and inversely proportional to density (ρ). SAR can be expressed as $\sigma|E|^2/\rho$ (Jia et al. 2017), where E is the electric field. A SAR level of 1.6 W/kg has been designated by the FCC as the limit of radio frequency energy that can be safely absorbed by humans (federal communications commission, 2011). The maximum value of SAR produced by C–C and C–S WPT systems are 0.25 W/kg and 0.29 W/kg respectively and therefore the optimized values obtained in the simulations at 13.56 MHz are safe and does not cause any tissue damage.

Step-8: End of inductive link optimization: The simulated results are validated using fabrication and experimental procedure. section 4 discusses the fabrication and measurement results of C–C and C–S WPT systems.

4. Measurement results and discussion

This section analyzes the fabrication and experimental results of C–C and C–S WPT systems at perfect alignment, lateral and/or angular misalignments. The PTE of the systems at air and tissue mediums are measured and compared.

In this paper, the copper coils are fabricated on the silicone plate as copper is compatible with silicone and can attain high Q-factor and this fabrication process is shown in Fig. 6(a). The first step of the fabrication process is to mould the silicon plates based on the coil sizes, followed by

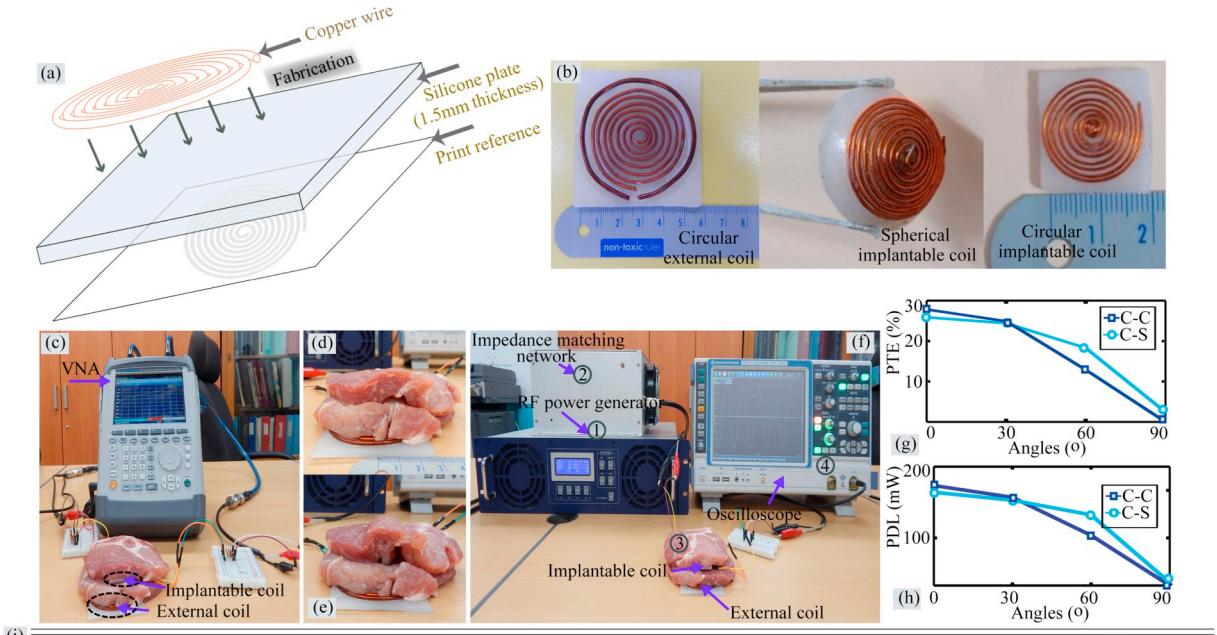

(i)

Reference	Type of wireless link	Coils shape	Implanted coil diameter (mm)	Operating frequency (MHz)	Distance (mm)	Medium	Measured PTE (%)
(Xue et al., 2013)	2-coil	Rectangular	25 × 10	13.56	10	Pork	58.2
(Sun et al., 2018)	4-coil	Circular	10.8 × 10.5	39.86	10	Pork	47.2
(Yang et al., 2017)	4-coil	Square	5 × 5	13.56	10	Pork	11.7
(Mirbozorgi et al., 2012)	3-coil	Circular	10.5	13.56	10	Beef	7
This work	3-coil	Spherical	18.8 × 5.4	13.56	10	Pork	26

Fig. 6. (a) Schematic illustration of coil fabrication process. (b) Circular shaped external coil with diameter of 5.5 cm, spherical shaped implantable coil with diameter and height of 1.88 cm and 0.54 cm respectively and circular shaped implantable coil with diameter of 1.87 cm. (c) Experimental setup for measuring the S-parameters between the coils. (d) Coils at lateral misalignment scenario. (e) Coils at angular misalignment scenario. (f) Experimental setup for measuring the power between the coils. (g) Measured PTE of C–C and C–S WPT systems from 0° to 90°. (h) Measured PDL of C–C and C–S WPT systems from 0° to 90°. (i) Comparison with conventional works.

fabricating the copper coils on the moulded silicone plate. A silicone plate with dimensions of 60 mm × 60 mm x 1.5 mm is used to design the external coil of C–C and C–S WPT systems and on the other hand a dimension of 20 mm × 20 mm x 1.5 mm is used to design the implantable coil of C–C WPT system. A spherical bowl with a height of 5.4 mm and outer diameter of 1.88 cm is moulded out of silicone material to design the implantable coil of the C–S WPT system. Fig. 6(b) shows the fabricated coils.

To analyze and measure the PTE of the 3-coil inductive C–C and C–S systems, in this paper, two types of experimental methods are employed. The first method works by measuring S_{21} at air and tissue mediums using an R&S ZVH4 vector network analyzer (VNA) (Jow and Ghovanloo, 2007). However, this method only measures the 3-coil inductive link efficiency and not the amount of power transferred. As shown in Fig. 6(c), the coils are placed parallel to each other separated by a distance of 10 mm. The port 1 of the VNA drives the primary side whereas the secondary side is driven by port 2, wherein both the ports have a default impedance of 50Ω. The PTE is computed based on the equation (3). At air medium, the PTE of C–C system is 35.4% and on the other hand C–S system produces a PTE of 33.8%.

To emulate the real time environment, a boneless pork sample with a thickness of 10 mm at 20° C is placed as a medium between the external and implantable coils and the setup is shown in Fig. 6(c). At this medium, at perfect alignment, the PTE of C–C and C–S WPT systems are 27.9% and 26% respectively. To measure the PTE at worst-case, coils are analyzed at a misaligned distance and misaligned angle of 10 mm and 90° respectively. Fig. 6(d) and (e) shows the lateral and angular misaligned scenarios respectively. The C–C WPT system shows a sharp decrease in PTE after 40° of angular misalignment when compared to C–S WPT system as predicted in the simulation. Fig. 6(g) shows the measured PTE of C–C and C–S WPT systems from 0° to 90°.

Generally, in biomedical implantable applications, the input power required for the external coil is extracted from the battery by the power amplifier or inverter. The AC power received by the external coil is transferred to the implantable coil wirelessly. As a DC voltage is required to operate the biomedical functional circuit, the AC power received by the implantable coil is converted to a DC voltage by a rectifier (Huang et al., 2018; Carta et al., 2011; Yan et al.2018). To set up this environment, the external coil is given an input of 1 W at 13.56 MHz through a RF power generator and the received power at the implantable side is calculated by directly measuring the voltage and current obtained through oscilloscope and power meter. The entire experimental setup is shown in Fig. 6(f). The actual power received by the implantable coil must be measured at both perfect and misalignment scenarios. When the coils are perfectly aligned in air medium, the actual power received by C–C and C–S WPT systems are 295 mW and 274 mW respectively. On the other hand, when the coils are perfectly aligned in tissue medium, the power received by C–C and C–S WPT systems at perfect alignment are 210 mW and 196 mW respectively. At 90° of angular misalignment, there is no power transfer between the external and implantable coils of C–C WPT system whereas the power received by C–S WPT system is 5.4 mW. This proves that C–S WPT system receives power even under the worst-case condition. Fig. 6(h) shows the measured PDL of C–C and C–S WPT systems from 0° to 90°. The proposed work is compared with the conventional works in tissue medium on the basis of WPT method type, frequency, implantable coil size, distance between the coils and PTE. The results are summarized as shown in Fig. 6(i).

5. Conclusion

In this paper, two 3-coil inductive WPT systems, having circular and spherical shaped implants are designed and compared to each other. The designs are simulated at 13.56 MHz and the distance between the external and implantable coils is 10 mm. The performance of the coils are tested at air and human tissue mediums. The system having spherical shaped implantable coil achieves a higher PTE under angular and a combination of angular and lateral misalignments. To validate the PTE of the designs generated by simulation, the simulated systems are analyzed by experimental method. A boneless pork sample with thickness of 10 mm is used as a medium to check the PTE between the coils in real-environment. Even in real-environment, the system with spherical shaped implant outperforms the system having circular shaped implant under misalignment cases. Future work implies to design a system by integrating the proposed design with small-sized integrated circuit to achieve a higher PTE.

Acknowledgments

This research was supported by the Basic Science Research Program through the National Research Foundation of Korea (NRF) funded by the Ministry of Education, Science and Technology (Grant No. NRF2016R1D1A3A03918084).

References

Agarwal, K., Jegadeesan, R., Guo, Y.-X., Thakor, N.V., 2017. Wireless power transfer strategies for implantable bioelectronics. IEEE Rev. Biomed. Eng. 10, 136–161.

Agrawal, D.R., Tanabe, Y., Weng, D., Ma, A., Hsu, S., Liao, S.-Y., Zhen, Z., Zhu, Z.-Y., Sun, C., Dong, Z., et al., 2017. Conformal phased surfaces for wireless powering of bioelectronic microdevices. Nature Biomed. Eng. 1 (3), 0043.

Ahn, D., Ghovanloo, M., 2016. Optimal design of wireless power transmission links for millimeter-sized biomedical implants. IEEE Trans. Biomed. Circuits Syst. 10 (1), 125–137.

Arbabian, A., Chang, T.C., Wang, M.L., Charthad, J., Baltsavias, S., Fallahpour, M., Weber, M.J., 2016. Sound technologies, sound bodies: medical implants with ultrasonic links. IEEE Microw. Mag. 17 (12), 39–54.

Carta, R., Tortora, G., Thoné, J., Lenaerts, B., Valdastri, P., Menciassi, A., Dario, P., Puers, R., 2009. Wireless powering for a self-propelled and steerable endoscopic capsule for stomach inspection. Biosens. Bioelectron. 25 (4), 845–851.

Carta, R., Thoné, J., Gosset, G., Cogels, G., Flandre, D., Puers, R., 2011. A self-tuning inductive powering system for biomedical implants. Procedia Eng. 25, 1585–1588.

Chatterjee, S., Iyer, A., Bharatiraja, C., Vaghasia, I., Rajesh, V., 2017. Design optimisation for an efficient wireless power transfer system for electric vehicles. Energy Procedia 117, 1015–1023.

Das, R., Yoo, H., 2015. Biotelemetry and wireless powering for leadless pacemaker systems. IEEE Microw. Wirel. Compon. Lett. 25 (4), 262–264.

Gong, F.-X., Wei, Z., Chi, H., Yin, B., Sun, Y., Cong, Y., Sun, M., 2017. Position and angular misalignment analysis for implantable wireless power transfer system based on magnetic resonance. J. Med. Biol. Eng. 37 (4), 602–611.

https://www.fcc.gov/general/body-tissue-dielectric-parameters.

Huang, C., Kawajiri, T., Ishikuro, H., 2018. A 13.56-mhz wireless power transfer system with enhanced load-transient response and efficiency by fully integrated wireless constant-idle-time control for biomedical implants. IEEE J. Solid State Circuits 53 (2), 538–551.

HG, L., JW, L., KW, S., JH, L., JH, C., 2009. A method for reducing body exposure to electromagnetic field of pillow type wireless charger in fully implantable middle ear hearing device. IEICE Electron. Express 6 (18), 1318–1324.

Jia, Y., Mirbozorgi, S.A., Wang, Z., Hsu, C.-C., Madsen, T.E., Rainnie, D., Ghovanloo, M., 2017. Position and orientation insensitive wireless power transmission for enercage-homecage system. IEEE Trans. Biomed. Eng. 10.

Jow, U.-M., Ghovanloo, M., 2007. Design and optimization of printed spiral coils for efficient transcutaneous inductive power transmission. IEEE Trans. Biomed. Circuits Syst. 1 (3), 193–202.

Karalis, A., Joannopoulos, J.D., Soljačić, M., 2008. Efficient wireless non-radiative mid-range energy transfer. Ann. Phys. 323 (1), 34–48.

Kassiri, H., Salam, M.T., Pazhouhandeh, M.R., Soltani, N., Velazquez, J.L.P., Carlen, P., Genov, R., 2017. Rail-to-rail-input dual-radio 64-channel closed-loop neuro-stimulator. IEEE J. Solid State Circuits 52 (11), 2793–2810.

Khan, S.R., Choi, G., 2016. Analysis and optimization of four-coil planar magnetically coupled printed spiral resonators. Sensors 16 (8), 1219.

Kiani, M., Jow, U.-M., Ghovanloo, M., 2011. Design and optimization of a 3-coil inductive link for efficient wireless power transmission. IEEE Trans. Biomed. Circuits Syst. 5 (6), 579–591.

Lee, H.-M., Park, H., Ghovanloo, M., 2013. A power-efficient wireless system with adaptive supply control for deep brain stimulation. IEEE J. Solid State Circuits 48 (9), 2203–2216.

Lenaerts, B., Puers, R., 2007. An inductive power link for a wireless endoscope. Biosens. Bioelectron. 22 (7), 1390–1395.

Mirbozorgi, S.A., Gosselin, B., Sawan, M., 2012. A transcutaneous power transfer interface based on a multicoil inductive link. In: 2012 Annual International Conference of the IEEE Engineering in Medicine and Biology Society. IEEE, pp. 1659–1662.

Mutashar, S., Hannan, M.A., Samad, S.A., Hussain, A., 2014. Analysis and optimization of spiral circular inductive coupling link for bio-implanted applications on air and within human tissue. Sensors 14 (7), 11522–11541.

Nguyen, M.Q., Hughes, Z., Woods, P., Seo, Y.-S., Rao, S., Chiao, J.-C., 2014. Field distribution models of spiral coil for misalignment analysis in wireless power transfer systems. IEEE Trans. Microw. Theory Tech. 62 (4), 920–930.

Poon, A.S., O'Driscoll, S., Meng, T.H., 2007. Optimal operating frequency in wireless power transmission for implantable devices. In: Engineering in Medicine and Biology Society, 2007. EMBS 2007. 29th Annual International Conference of the IEEE. IEEE, pp. 5673–5678.

RamRakhyani, A.K., Mirabbasi, S., Chiao, M., 2011. Design and optimization of resonance-based efficient wireless power delivery systems for biomedical implants. IEEE Trans. Biomed. Circuits Syst. 5 (1), 48–63.

Soma, M., Galbraith, D.C., White, R.L., 1987. Radio-frequency coils in implantable devices: misalignment analysis and design procedure. IEEE Trans. Biomed. Eng. (4), 276–282.

Stingl, K., Bartz-Schmidt, K.U., Besch, D., Braun, A., Bruckmann, A., Gekeler, F., Greppmaier, U., Hipp, S., Hörtdörfer, G., Kernstock, C., et al., 2013. Artificial vision with wirelessly powered subretinal electronic implant alpha-ims. Proc. R. Soc. Biol. Sci. 280 (1757), 20130077.

Vijayakumaran Nair, V., Choi, J.R., 2016. An efficiency enhancement technique for a wireless power transmission system based on a multiple coil switching technique. Energies 9 (3), 156.

W federal communications commission, 2011. Specific Absorption Rate (Sar) for Cellular Telephones. [online] available: https://www.fcc.gov/general/specific-absorption-rate-sar-cellular-telephones.2013.

Yan, X.-Y., Yang, S.-C., He, H., Tang, T.-Q., 2018. An optimization model for wireless power transfer system based on circuit simulation. Phys. A Stat. Mech. Appl. 509, 873–880Elsevier.

Yellappa, P., Lee, Y.R., Choi, J.R., 2018. Analysis of coil misalignment issue in resonance-based wireless power transmission system for implantable biomedical applications. In: Circuits and Systems (ISCAS), 2018 IEEE International Symposium on. IEEE, pp. 1–5.

Zhang, J., Yuan, X., Wang, C., He, Y., 2017. Comparative analysis of two-coil and three-coil structures for wireless power transfer. IEEE Trans. Power Electron. 32 (1), 341–352.

Zhong, W., Zhang, C., Liu, X., Hui, S.R., 2015. A methodology for making a three-coil wireless power transfer system more energy efficient than a two-coil counterpart for extended transfer distance. IEEE Trans. Power Electron. 30 (2), 933–942.